THE TDR HELICOPTER CONCEPT : DESIGN AND INTEGRATION OF THE LJUNGSTRÖM TURBINE

Frank Buysschaert, Simon Newman, Scott Walker, University of Southampton, Southampton, United Kingdom
Patrick Hendrick, Université Libre de Bruxelles, Brussels, Belgium
Hubert Antoine, SAGITA SA, Wandre, Belgium

Abstract

This paper examines the design of a rotor embedded Ljungström turbine (RELT) and its integration in the TDR helicopter cycle, with the objective to maximise the performance gain of the TDR helicopter with respect to conventional single rotor helicopters. For this purpose, a RELT turbine model is discussed briefly and applied to a 500 kg VLR- and a 10 metric ton NH-90-class TDR helicopter in nominal operation conditions ISA SLS. In this study, the coefficient of performance margin is vital. The VLR-class TDR helicopter, using either an Avgas or a Diesel reciprocating engine of approximately 90 kW, exhibits a performance gain of circa 10% over the conventional helicopter. The NH-90-class TDR helicopter benefits from an impressive coefficient of performance margin of 47% while using a turbofan with a thrust potential of 22.5 kN, which makes the concept attractive in the heavy helicopter category. For both configurations, a RELT geometry is proposed yielding adequate turbine polytropic efficiencies between 85% and 90%.

1. INTRODUCTION

The Turbine Driven Rotor (TDR) concept is a helicopter configuration using coaxially placed rotors driven directly by a Ljungström turbine embedded in the rotor head (Fig.1). It benefits from the absence of both a mechanical transmission system and a tail rotor. The latter components were shown to increase the helicopter operating costs and give rise to safety and performance concerns[1]. The TDR concept was firstly introduced by Antoine et al.[2] and subsequently studied by Buysschaert et al.[3,4] and exhibits a noteworthy performance potential over the conventional single-rotor helicopter. This paper builds further on the previous observations and discusses the design and integration of the Ljungström turbine in two helicopter types. The first helicopter type is a VLR[1]-class helicopter of 500 kg using a piston engine as cycle power source. The second helicopter type is a NH-90-class helicopter, using a turbofan as cycle power source. Both TDR helicopters are then compared to their respective conventional equivalents. This study focusses on maximum power operating conditions at sea level ISA only.

Fig.1 : TDR Ultra-light concept of Sagita S.A.

[1] Very Light Rotorcraft

2. CYCLE PRESENTATION AND THERMODYNAMIC CHARACTERISATION

Finding the required engine power P_M^* for a conventional helicopter is straightforward, since there is a mechanical link between the engine and all rotors. This is not possible in case of the TDR helicopter. The rotor embedded Ljungström turbine (RELT) driving the rotors is mechanically disconnected from the engine. The power the latter delivers P_T^* is therefore not necessarily equal to the power generated by the RELT. Buysschaert et al.[4] proposed the coefficient of performance (*COP*) to quantify this difference, where :

$$(1) \qquad COP = \frac{P_T^*}{P_M^*}$$

COP can be larger than unity, depending on the selected cycle parameters. The cycle parameters should be selected such that a satisfactory coefficient of performance is achieved for the intended application. The cycle used for respectively the VLR-class and the NH-90-class TDR helicopters is presented next.

2.1. The piston engine powered TDR cycle

Buysschaert et al.[4] presented the piston engine powered TDR cycle as ideal for the low power class TDR helicopter. For the intended weight category, it is sensible to expect an installed engine power below 100 kW, as can be found comparing helicopters of a similar weight category (for example the Robinson R22). Fig.2 explains the modus operandi of the piston engine (PE) powered TDR

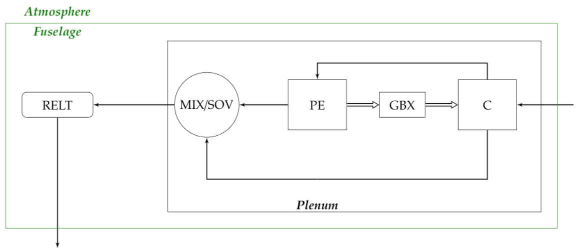

Fig.2 : Piston engine powered TDR cycle.

cycle schematically. Air enters a compressor (C), which is placed in a pressurised vessel or *plenum*, installed in the fuselage of the helicopter. The compressor is driven by a piston engine (PE), which is mechanically connected to the latter by shafts and, if necessary, a gearbox (GBX). The engine is positioned in the plenum and ingests pressurised air, provided by the compressor. Only part of the flow leaving the compressor enters the engine. The remaining flow bypasses and cools the engine, and is eventually mixed (MIX) with the exhaust gases of the piston engine, prior to being expanded in the RELT. The shut-off valve (SOV) disconnects the flow path from the RELT, in case of a system failure.

The coefficient of performance of such a cycle may be proven to be :

$$COP \approx \eta_M \frac{T_{t45}}{T_{t1}} \frac{1-\left(\frac{1}{\pi_C}\right)^{\frac{\gamma_g-1}{\gamma_g}\eta_{p,T}}}{\pi_C^{\frac{\gamma-1}{\gamma}\frac{1}{\eta_{p,C}}}-1} \tag{2}$$

where η_M the mechanical efficiency of the transmission system, π_C the cycle total-to-total pressure ratio and here assumed equal to the RELT total-to-total expansion ratio. T_{t45} and T_{t1} are respectively the RELT inlet temperature and the compressor total inlet temperature. $\eta_{p,T}$ and $\eta_{p,C}$ are respectively the polytropic turbine and compressor efficiencies. Examination of Eq.2 shows that *COP* is maximised when, for a given inlet temperature, the Ljungström turbine inlet temperature (*LTIT*, i.e. T_{t45}) is high and the pressure ratio low. With regard to the polytropic efficiencies, it is obvious that they should be as high as possible. For a more detailed examination of the cycle, the reader is referred to Buysschaert et al.[4]. The foregoing conclusion is sufficient for the currently conducted discussion.

2.2. Turbofan powered TDR cycle

Based on the required engine power at take-off for the NH-90 helicopter, which is over 3 MW, it is clear that the turbofan powered TDR cycle is the preferred candidate to drive the rotors of the TDR helicopter in the considered weight category[4].

The turbofan is a low-total-pressure and low-total-temperature gas generator, with the prime objective to deliver thrust to an aircraft. However, in case the nozzle is replaced by the RELT, the turbofan engine is capable of conditioning the gases such that high RELT power levels can be achieved. A schematic representation of the turbofan powered TDR cycle is adopted in Fig.3. It represents a twin-turbofan configuration, with thrust valves (TV), enabling a part of the exhaust gases to expand

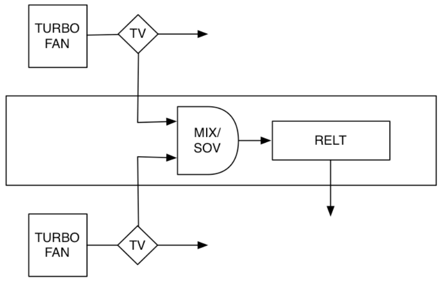

Fig.3 : Turbofan engine powered TDR cycle. Twin-turbofan engine configuration

through a nozzle instead of the RELT, which results in the generation of a propulsive force like the World Speed Record Lynx. This thrust force can be used in case compounding is pursued. For the work at hand, only a single turbofan configuration without compounding will be assessed (closed thrust valves).

When the flight velocity is neglected, it is possible to define a coefficient of performance for the turbofan powered TDR cycle, based on the kinetic energy increase the turbofan can deliver. From Buysschaert et al.[4] :

$$COP_{TF} = \frac{2}{SPT^2/T_{t1}}\left[C_p + \frac{FAR/T_{t1}}{(1+BPR_{TF})}LHV\eta_{CC}\right]\cdots \left[1-\left(\frac{1}{\pi_F}\right)^{\frac{(\gamma_g-1)}{\gamma_g}\eta_{p,T}}\right] \tag{3}$$

SPT is the turbofan specific thrust, C_p the specific heat of air at constant pressure, *FAR* the fuel-to-air ratio, BPR_{TF} the selected turbofan bypass ratio, *LHV* the fuel lower heating value, η_{CC} the combustion chamber efficiency, π_F the fan total-to-total pressure ratio, γ_g the exhaust gas specific heat exponent and $\eta_{p,T}$ the RELT polytropic efficiency. Relying again on the findings stated in Buysschaert et al.[4], it is possible to show that the cycle coefficient of performance increases while selecting a high bypass ratio and fan pressure ratio.

2.3. Conclusion

At this point, the reader should note that the interrelationship between the RELT polytropic efficiency and the turbine inlet total temperature/pressure conditioned by the cycle has not been examined yet. This requires a model of the RELT to be established first, such that the impact of the cycle pressure, temperature and mass flow on the turbine polytropic efficiency is determinable. The next section discusses this topic.

3. LJUNGSTRÖM TURBINE DESIGN AND EFFICIENCY OPTIMISATION

Buysschaert et al.[3] already discussed the blade passage characteristics of the RELT, but did not include the disk friction and leakage losses. Also, for design purposes, the therein-reported model still has too many degrees of freedom, which is undesirable. Here, some important RELT design aspects will be reported qualitatively, which enable the designer to find a configuration with satisfying efficiency characteristics. The design criteria are established for nominal operating conditions.

3.1. Velocity triangles

The air extracted from the plenum enters the RELT radially (Fig.4), i.e. with negligible tangential velocity component. From an efficiency perspective, it is interesting to avoid a tangential speed component of the gases leaving the RELT as well, as this kinetic energy cannot be recovered. In addition, the workload per stage should be well balanced, as it is related to the flow deflection ε, which impacts the aerodynamic losses significantly. ε should be minimised as the aerodynamic stage losses are proportional to ε^2, as explained by the model of Soderberg[5]. It is therefore sensible to distribute ε evenly over each stage, and thus keep the velocity triangles invariant throughout the turbine, except for the first and last stage, which have to cope with the imposed radial flow conditions and the absolute inlet and outlet flow angles of respectively the second and penultimate stage. Note that from now on, all stages in between the first "^{1}" and last "^{L}" stages will be designated as the middle stages "^{M}", over which the velocity triangles are set equal (Fig.5).

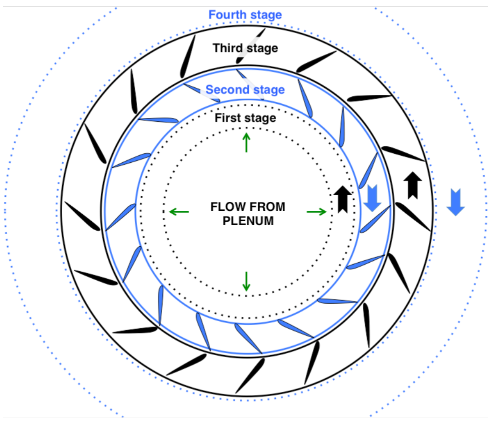

Fig.4 : RELT radial inflow condition.

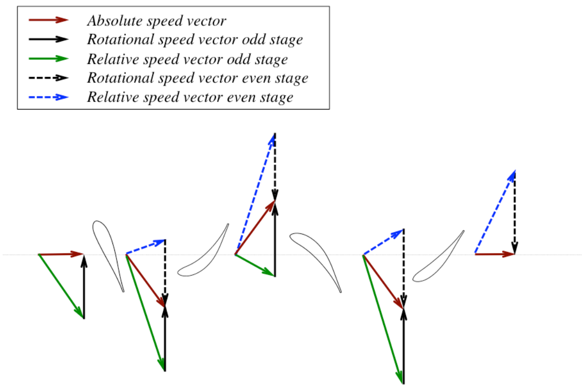

Fig.5 : Stage velocity triangles - conservation of the absolute and relative flow angles (4-stage turbine).

Based on the above discussion, it is possible to prove that, by approximation, the blade passage work coefficient $^M\psi$ over the middle stages is constant :

$$^M\psi = 2 \cdot {}^M\phi_i \tan({}^M\alpha_i) \tag{4}$$

and is twice the blade passage work coefficient found over the first and last stages :

$$^1\psi = {}^L\psi = {}^M\phi_i \tan({}^M\alpha_i) \tag{5}$$

$^M\alpha_i$ is the absolute flow angle at any middle stage inlet (Fig.6) and $^M\phi_i$ the middle stage flow coefficient. Note that, by definition :

$$\psi \triangleq \frac{h_{ti} - h_{to,b}}{u_i^2} \tag{6}$$

and,

$$\phi_i = \frac{v_{iR}}{u_i} \tag{7}$$

The suffix "*i*" and "*o*" respectively stand for the inlet and outlet conditions, while suffix "*b*" refers to the blade passage. u_i is the rotational speed at the inlet of the blade passage, v_{iR} the radial component of the absolute speed at the inlet of the blade passage and "h_t" the specific total enthalpy of the gases.

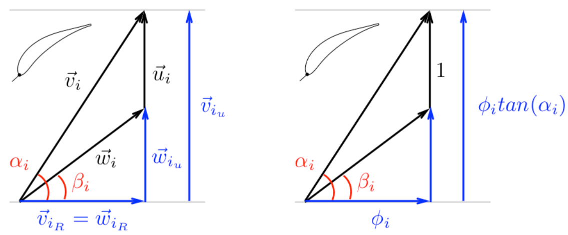

Fig.6 : Stage inlet velocity triangle

The flow deflection over the middle stages $^M\varepsilon$ is a pure function of $^M\alpha_i$ and $^M\phi_i$:

$$\tan({}^M\epsilon) = \frac{2\tan({}^M\alpha_i){}^M{\phi_i}^2}{[1 - \tan^2({}^M\alpha_i)]{}^M{\phi_i}^2 + 1} \tag{8}$$

$^M\varepsilon$ generally increases with $^M\alpha_i$ and $^M\phi_i$, and can be shown to be higher than the deflection in the first and the last stage, but this discussion is not conducted here.

3.2. Blade passage losses

In Buysschaert et al.[3] the blade passage losses were established using the updated model of Ainley and Mathieson[6]. This model becomes too involved and not practical for a design process, in which many geometric parameters still need to be determined. As a consequence, the model of Soderberg was used, which - for nominal operating conditions and the optimum blade spacing criterion - yields satisfactory results, while requiring much less input data[5]. The model includes the effects of profile and secondary losses, and corrects for variations in blade aspect ratio and flow Reynolds number. In turbines, the aerodynamic losses are typically represented by a non-dimensional enthalpic loss ζ_A. This parameter is defined as :

$$(9) \qquad \zeta_A \triangleq \frac{h_{tL}}{u_o^2}$$

where Δh_{tL} is the specific total enthalpy rise due to the blade passage losses and u_o the rotational velocity ruling at the blade outlet. Based on conservation of mass, the definition of blade aspect ratio and Reynolds number, and use of the optimum pitch-to-chord ratio following Zweifel[13], it is possible to show that for the considered Ljungström turbine configuration the following relation stands :

$$(10) \qquad \zeta_A = f\left(\frac{1}{\dot{m}}, \Omega_C, R_i, \frac{R_o}{R_i}, {}^{M}\phi_i, {}^{M}\alpha_i\right)$$

where R_i the stage inlet radius, $\dot{m}$, the mass flow passing through the stage, Ω_C the turbine stage angular speed, and, ϕ_i and α_i respectively the stage inlet flow coefficient and absolute flow angle. Note the importance of the stage outlet-to-inlet radius ratio R_o/R_i, which has a significant impact on the turbine blade chord.

3.3. Blade geometry selection

For the work at hand, the blade profile is selected by means of the stage reaction degree $\hat{R}$, which is defined as :

$$(11) \qquad \hat{R} = 1 - \frac{P_A}{P_{st,b}} = 1 - \frac{\frac{v_i^2 - v_{o,b}^2}{2}}{h_{ti} - h_{to,b}}$$

P_A and $P_{st,b}$ are respectively the active and the total power generated in the blade passage. v is the absolute speed. With respect to the RELT, the reaction degree for the first, middle and last stages can be proven to be :

$$(12) \qquad {}^{1}\hat{R} = 1 + \frac{{}^{M}\phi_i \ \tan({}^{M}\alpha_i)}{2} \quad > 1$$

$$(13) \qquad {}^{M}\hat{R} = 1$$

$$(14) \qquad {}^{L}\hat{R} = 1 - \frac{{}^{M}\phi_i \ \tan({}^{M}\alpha_i)}{2} \quad < 1$$

The foregoing equations uncover that all but the last stage operate at a reaction degree of at least 1. In this paper, the NACA A_3K_7 profile is selected for the RELT turbine (Fig.7), which is according to Horlock[5] suitable for *reaction* blades, where an acceleration of the flow in the blade passage is realised. In general, the RELT turbine responds to this criterion. It is noted that the last stage might benefit from a different profile developed for a turbine stage wherein the acceleration occurs in a lesser degree, but this is part of future research. A standard thickness-to-chord ratio of 20% was adopted.

3.4. Disk friction and leakage losses

With respect to conventional turbines used in an aero-engine, the radius of the RELT can be large. Hence, the effects of disk friction may rise to unacceptable levels. At the same time, leakage losses exist and need to be assessed. Also, there is no stator in the Ljungström turbine. This affects the power balance, which thus needs to be treated differently than what is proposed by the models used for axial turbines.

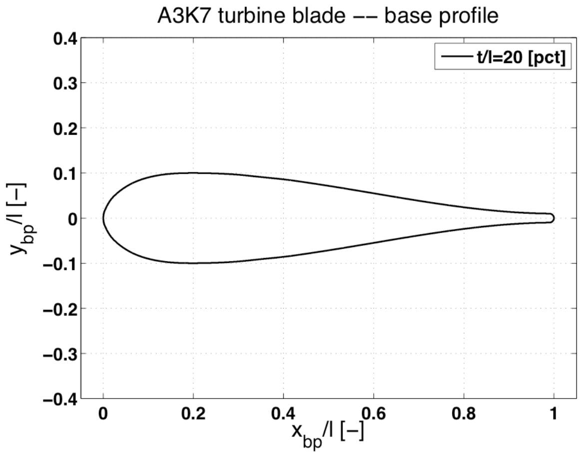

Fig.7 : A_3K_7 base profile

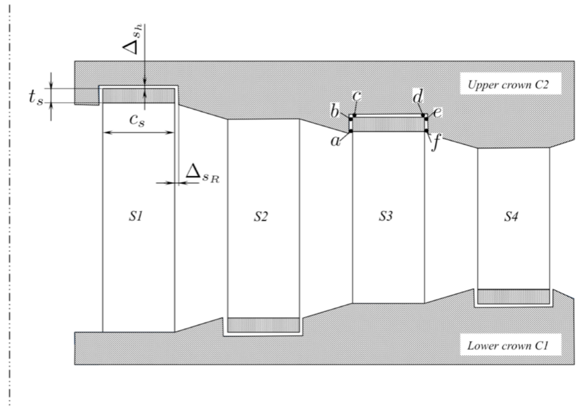

Fig.8 : Vertical cross-section of a 4-stage RELT

The study quantifying the disk friction losses includes three viscous loss types. Here, they are represented by a non-dimensional enthalpic loss ζ_{FL}, which is defined as :

$$(15) \qquad \zeta_{FL} \triangleq \frac{\Delta h_{t_{FL}}}{u_o^2}$$

where Δh_{tFL} is the flow specific total enthalpy rise due to the viscous losses. In the subsequent studies, the non-dimensional enthalpic losses will be expressed as functions of important dimensional and non-dimensional design parameters. Note that full non-dimensional parameters could have been used instead, but this would render the analysis of the problem more difficult.

The first viscous loss type is torsional Couette flow, occurring in the space between the rim of a stage and the opposing disk in which it revolves (Fig.8, section c-d). Following the works of Daily and Nece[7,8], and Goulburn and Wilson[9], it was possible to derive an optimum dimension for the axial spacing Δ_{s_h} (minimum friction), which depends entirely on the stage outlet radius R_o :

(16) $\Delta_{s_h}/R_o \in [0.0124; 0.02]$

The non-dimensional enthalpic losses provoked by the torsional Couette flow $\zeta_{FL_{TOC}}$ can be shown to be proportional to :

(17) $$\zeta_{FL_{TOC}} \propto \left(R_i, \frac{R_o}{R_i}, \frac{1}{\dot{m}}\right)$$

Secondly, a Taylor-Couette flow is found in sections (a-b) and (e-f) (Fig.8), and represents the flow between coaxially placed revolving cylinders. Quantifying the friction produced by this flow type is difficult due to flow instabilities, especially when the imposed radial play is small with respect to the cylinder radii[10], i.e. :

(18) $\Delta_{s_R} << R_{i/o}$

This condition applies in the case of the RELT. The losses may then be estimated locally by planar Couette flow[10,11]. As a consequence, and similar to the torsional Couette flow, one may prove that the non-dimensional enthalpic loss related to the Taylor-Couette flow in the turbine $\zeta_{FL_{TAC}}$ is proportional to :

(19) $$\zeta_{FL_{TAC}} \propto \left(R_i, \frac{R_o}{R_i}, \frac{1}{\dot{m}}\right)$$

Thirdly, the viscous losses in the labyrinth seals integrated in sections (a-b) and (e-f) cannot be neglected. According to Eser and Dereli[12], the losses in the cavity can be approximated by considering turbulent flow to circulate in a duct formed by the disk and the notch in the rim (Fig.9) at an average speed v_{cav}, where :

(20) $v_{cav_{i/o}} \approxeq \Omega_C \; R_{i/o}$

Ω_c is the angular velocity of either rim or disk, and assumed equal in case of nominal operating conditions. Note that the rim is notched at both sides, which needs to be accounted for separately. Naturally, the area affected by the cavity in sections (a-b) and (e-f) is subtracted from the area to which Taylor-Couette flow is applied. The non-dimensional enthalpic loss due to the presence of the labyrinth seals can then be demonstrated to be commensurate with :

(21) $$\zeta_{FL_{CAV}} \propto \left(R_i, \frac{R_o}{R_i}, \Omega_C, \frac{1}{\dot{m}}\right)$$

The leakage losses in the Ljungström turbine were examined by considering the space between rim and opposing disk (Fig.9) to resemble a see-through labyrinth seal. Malvano et al.[14] and Eser & Kazakia[15] then propose to use the model of Neumann[16] to calculate the leakage mass flow. A parametric study consequently showed that the amount of labyrinth seals (N_{ss}) set equal to 4 gives a satisfactory reduction in leakage mass flow, while offering the manufacturer sufficient margin on the selection of the labyrinth seal dimensions w_{ss_j}, h_{ss_j} and L_j (Fig.9). With regard to the RELT, using this model uncovers that the leakage losses will be less than 1% of the mass flow passing through the stage. For design purposes, it is then reasonable to neglect the leakage losses.

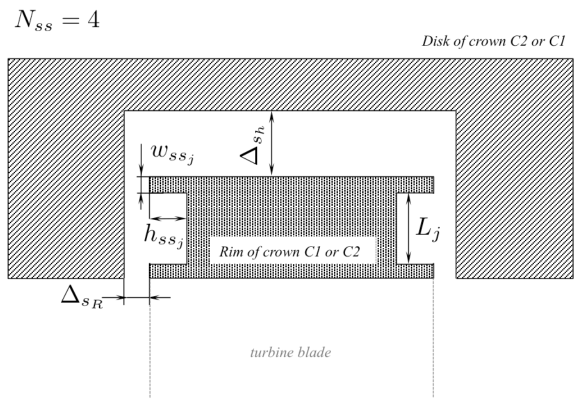

Fig.9 : RELT labyrinth seal configuration

3.5. Loss trade-off study

As an approximation, the middle stage flow coefficient is expressed by :

(22) $${}^{M}\phi_{i_{Ops}} \approxeq \frac{{}^{1}\hat{\theta}\left(1-\pi_T^{\frac{1-\gamma}{\gamma}\eta_{p,T}}\right)}{2(S_n-1)\tan{}^{M}\alpha_i}$$

where ${}^{1}\hat{\theta}$ is the first stage non-dimensional total inlet enthalpy and equal to ${}^{1}h_{ti} / {}^{1}u_i^2$, while S_n represents the number of stages. Note that the cycle pressure ratio π_C is à priori imposed by the designer's wish to maximise *COP*. A reasonable approximation is to consider the turbine expansion ratio to be constant and more or less equal to the cycle pressure ratio ($\pi_T \cong \pi_C$). Since for a given configuration and cycle operating point S_n, π_T and ${}^{M}\alpha_i$ are determined, and, near the optimum operating point $\eta_{p,T}$ more or less invariant, it is found that, using Eq.22 :

(23) $${}^{M}\phi_{i_{Ops}} \propto \frac{1}{\Omega_C^2 \; {}^{1}R_i^2}$$

From Eq.17, Eq.19 & Eq.21 it is evident that Ω_C and ${}^{1}R_i$ should be minimised for minimum losses. However, Eq.10 in turn indicates that for the same reason ${}^{M}\phi_i$ must be kept low as well. Yet, according to Eq.23, this is not possible. Selecting a low Ω_C and ${}^{1}R_i$ will yield a high ${}^{M}\phi_i$ and vice versa. This behaviour uncovers the existence of an optimum that will result in a minimum loss and maximum efficiency. The previously mentioned optimum will be used later in this paper.

A sensitivity study on this trade-off study using various inlet radii, angular speeds, outlet-to-inlet radius ratios, mass flows, cycle pressure ratios and number of stages, showed that the optimum ${}^{M}\alpha_i$ is generally found around 65°. This "high" value allows the designer to reduce ${}^{M}\alpha_i$ slightly in case the blade height is too important, without a significant loss penalty (Section 4.5.2).

Note that in case of a helicopter, the rotor tip radius R_T depends on helicopter gross weight, while an average main rotor blade tip speed of 215 m/s is to be adopted[1]. By definition :

$$\text{(24)} \qquad \Omega_C\ {}^1R_i = v_{tip}\left(\frac{{}^1R_i}{R_T}\right) = v_{tip}\ \bar{r}_i \quad \text{and} \quad \bar{r}_i \triangleq \frac{{}^1R_i}{R_T}$$

where $\bar{r}_i$ is the RELT specific inlet radius. Substitution of the above in Eq.22 :

$$\text{(25)} \qquad {}^M\phi_{i_{Ops}} \propto \frac{1}{\bar{r}_i^2}$$

Based on the foregoing discussions, an optimum RELT specific inlet radius appears determinable, for which the efficiency is maximised.

4. TDR CYCLE AND TURBINE MATCHING

4.1. Break-even Coefficient of Performance

In the previous sections, some important performance-driving aspects of the TDR cycles and the RELT were discussed briefly. At this point, it is interesting to tune both systems such that the TDR helicopter benefits from a maximum performance gain with regard to the conventional helicopter. In order to attain this, a performance metric needs to be developed such that a comparison between the TDR helicopter and its conventional counterpart is made possible. The break-even coefficient of performance COP_{BE} serves this purpose.

A TDR helicopter is stated to perform as good as its conventional counterpart when, for a given flying time and performance setting, it consumes an equal amount of fuel. The fuel consumption will be function of the flight profile, but at this point, the performance characteristics will be examined in abstraction from this issue and a constant fuel consumption is adopted for the dominant flight regime. As a consequence :

$$\text{(26)} \qquad \dot{m}_{f,TDR}\Delta t_{flight} = \dot{m}_{f,conv}\Delta t_{flight}$$

$$\text{(27)} \qquad \dot{m}_{f,TDR} = \dot{m}_{f,conv}$$

For a given rotor power requirement, the condition stated in Eq.27 imposes a certain value to the cycle specific fuel consumption SFC_{TDR}. This concurs with the cycle operating at a particular coefficient of performance This coefficient of performance is the break-even coefficient of performance. From the definition of the specific fuel consumption of an internal combustion engine SFC_E, i.e. :

$$\text{(28)} \qquad SFC_E = \frac{\dot{m}_f}{P_M^*}$$

and the definition of COP (Eq.1), it is possible to develop the following relation for the break-even coefficient of performance :

$$\text{(29)} \qquad COP_{BE} = \frac{SFC_{E,TDR}}{SFC_{E,conv}}\frac{P_T^*}{P_{M,conv}^*}$$

$P^*_{M,conv}$ is the installed engine power in the conventional helicopter. The power delivered by the RELT is only necessary to drive the coaxial rotors. Unlike the conventional helicopter, no mechanical transmission losses or tail rotor power needs to be provided. Also, the conceptual difference causes a change in platform empty weight. In a conventional helicopter, the required engine power may be expressed as function of gross weight using a power function $P^*_{M,conv} = a \times W_g^b$, which is illustrated by the trend-line in Fig.10, for which a=0.068 and b=1.1693. Taking the previously mentioned aspects of a change in empty weight and power demand into account, it is possible to write :

$$\text{(30)} \qquad \frac{P_T^*}{P_{M,conv}^*} = \left(1 + \frac{\Delta W_E}{W_{g,conv}}\right)^b (1 - k_{TX} - k_{TR})\ k_I$$

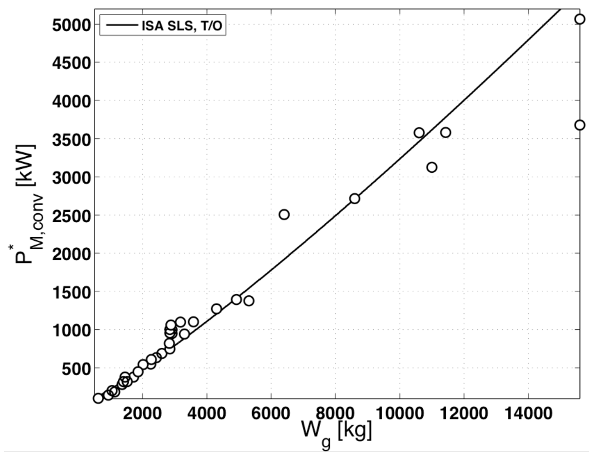

Fig.10 : Installed maximum take-off power (ISA SLS) Turboshaft engine(s) [1]

k_{TX} and k_{TR} are the fractions of the installed engine power dissipated in respectively the transmission system and the tail rotor. ΔW_E is the increase in empty weight of the TDR helicopter with respect to the conventional platform. k_I is a correction term that accounts for the increase in power consumption due to the presence of the RELT in the rotor head (reduced rotor disk area with respect to the conventional helicopter). Note that Eq.30 was established on the assumption that for similar rotor disk loadings, the engine power consumption in a single-rotor helicopter and a coaxial-rotor helicopter is identical[17]. A reduction of the rotor disk area consequently results in an increase in rotor power demand, which needs to be accounted for. However, since the used design procedure imposes that $R_{T,TDR} = R_{T,conv}$, while in general ΔW_E is negative and thus the gross weight of a TDR helicopter is lower than the conventional helicopter, an important change in disk loading will not be expected, even though the rotor disk area is reduced. Hence by approximation : k_I = 1.

Eq.29 clearly highlights that P^*_T / $P^*_{M,conv}$ should be low. The lower COP_{BE} the worse the TDR cycle characteristics may be to yield the same performance as the conventional helicopter. The ratio of the engine specific fuel consumptions in Eq.29 is also of significant importance. It is engine-type dependent. Note that Eq.29 will be modified when a turbofan is used, since the latter does not deliver power on a shaft directly, but thrust instead.

TABLE 1 : POWER REDUCTION FACTORS

k_{TX} [-]	0.04 ... 0.09	[18,19]
k_{TR} [-]	0.05 ... 0.10	[18,19]
k_I [-]	1.00	-

4.2. COP-margin

The COP-margin COP_M presents the "goodness" of the cycle coefficient of performance with respect to the the break-even coefficient of performance and is an ideal yardstick to evaluate the performance potential a TDR helicopter has over a conventional helicopter. By definition :

$$COP_M \triangleq \frac{COP - COP_{BE}}{COP_{BE}} \tag{31}$$

This parameter will be used in the subsequent cycle design study.

4.3. Engine regime setting

The reader is noted that for the subsequent study, which matches the cycle and turbine characteristics, the engine setting for both the piston engines and the turbofan is the maximum power/thrust setting. This because the RELT is then operating at its maximum inlet temperature (*LTIT*), which is for reasons of rotor head bearing integrity limited to 400 K[4]. In addition, for the previously mentioned engine regime, performance data is made readily available by the engine manufacturer. While this operating regime is usually not the design criterion of importance in the considered flight profile, it will be used here to obtain a first evaluation of the TDR helicopter design characteristics.

4.4. VLR piston engine powered TDR cycle

4.4.1. Estimation of COP_{BE}

From Eq.29 it is observed that the piston engine installed in the TDR cycle should have an as low as possible SFC_E.

TABLE 2 : SELECTED VLR-CLASS TDR HELICOPTER PE $SFC_{E,TDR}$

Avgas engine	250	[g/kWh]
Diesel engine	230	[g/kWh]

Based on the data described in Fig.11, the four-stroke atmospherically blown piston engine (Avgas) and the two-stroke Diesel engine appear to have the lowest specific fuel consumption. These are consequently retained for the design cycle study (Table 2).

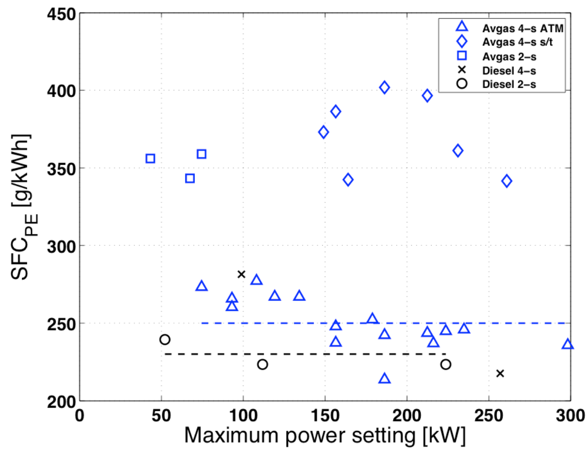

Fig.11 : Piston engine SFC at maximum engine rating (ISA SLS, from author survey)

In the low power class helicopter niche (<100 kW), it is not unusual to find a piston engine installed in the conventional helicopter as well. Hence, in a first approximation $SFC_{E,TDR} = SFC_{E,conv}$ and as a consequence, only the empty weight variation ΔW_E between the TDR concept and the conventional helicopter remains to be determined :

$$\Delta W_E \approxeq W_{E,T} + W_{E,C} + \Delta W_{E,2} - W_{E,3A} - W_{E,7B} \tag{32}$$

$W_{E,T}$ is the weight added due to the installation of a RELT in the rotor head, $W_{E,C}$ is the weight of the compressor (Fig.2), $\Delta W_{E,2}$ the change in weight by using a coaxial rotor instead of a single rotor configuration, $W_{E,3A}$ the weight of the tail rotor system and $W_{E,7B}$ the weight of the transmission system. The latter two weight categories are subtracted from the weight balance, as they are nonexistent in the TDR helicopter. All weight correlations are based on the model of Beltramo & Morris[20], except for $W_{E,T}$ and $W_{E,C}$, which were estimated on the weight fractions of the TDR prototype developed by Sagita S.A. and which are reflected in Table 3.

For a VLR-class TDR helicopter of 500 kg, it was then found that (Fig.12) :

$$\frac{\Delta W_E}{W_{g,conv}} \approxeq -0.14 \tag{33}$$

From Eqs. 29 & 30, COP_{BE} for both PE cycles (Avgas & Diesel) then shows to be :

$$COP_{BE} \approxeq 0.721 \tag{34}$$

The integrated cycle and turbine design methodology will yield a value for *COP*, which makes the determination of COP_M possible. This is discussed next.

TABLE 3 : TDR HELICOPTER TURBINE AND COMPRESSOR SYSTEM WEIGHT FRACTIONS (ESTIMATIVE VALUES)

$W_{E,T} / W_{g,conv}$	0.061	[-]
$W_{E,C} / W_{g,conv}$	0.013	[-]

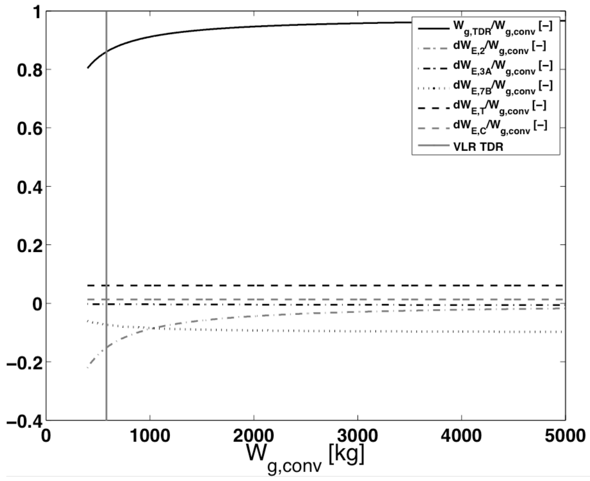

Fig.12 : PE Powered TDR helicopter empty weight fractions and variation.

4.4.2. Cycle and turbine matching

Thanks to empty weight study, it is possible to find the equivalent conventional helicopter gross weight, which is 581 kg. Eq.30 then allows retrieving the required RELT power P_T, which equals 83.7 kW in total, i.e. approximately 41.9 kW per turbine half (or crown - Fig.8). The impact of the RELT inlet temperature *LTIT* on COP_M is assessed parametrically. Buysschaert et al.[4] proved that for a given piston engine SFC_E, the cycle pressure ratio becomes a pure function of *LTIT*. The evolution of cycle pressure ratio with *LTIT* is shown in Fig.13 for the examined piston engine types. As explained by Buysschaert et al.[4], the cycle pressure ratio increases in case a higher *LTIT* is selected. The reason for this relationship is found with the increased available engine power per unit mass flow, caused by the fixed SFC_E and the increase in the fuel flow mass fraction. The latter is necessary in order to achieve higher values of *LTIT*. The rise in engine power availability per unit mass flow consequently demands for a higher cycle pressure ratio in order to match the mechanical power balance. For a more detailed discussion, the reader is referred to the work of Buysschaert et al.[4].

In Section 3.5, it was already mentioned that the rotor tip speed is considered helicopter type independent in the conducted study. The rotor radius is chosen by means of the empirical correlation of Buysschaert et al.[1], and is R_T=3.2 m. The rotor rotational speed then is approximately 655 RPM.

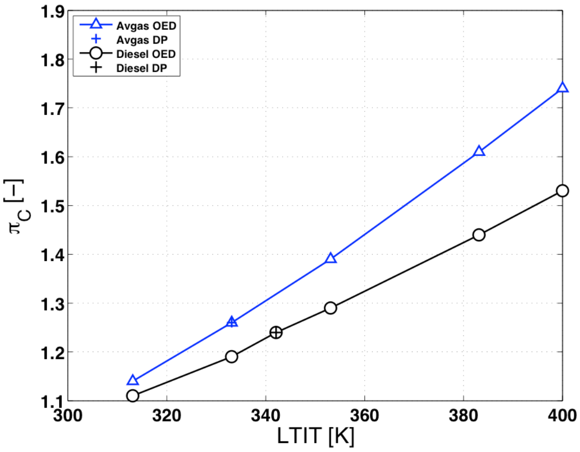

Fig.12 : Cycle pressure ratio as a function of RELT inlet temperature.

Following the loss trade-off study discussed briefly in Section 3.5 and knowing the required power demand, it is possible to find the optimum RELT specific inlet radius $\bar{r}_{i,opt}$ where the turbine efficiency is maximised. This is further referred to as "OED" or Optimum Efficiency Design. It can be shown that *LTIT* has a negligible impact on $\bar{r}_{i,opt}$ (proof is not delivered here). However, this cannot be concluded for a variation in the number of turbine stages S_n, which influences the stage work coefficient substantially. In general, an increase in the number of stages, improves the isentropic turbine efficiency for the same power output. Table 4 summarises the findings of the parametric study on $\bar{r}_{i,opt}$, using the number of stages as the independent variable. From Table 4 it may then be observed that for both piston engine types, 6 turbine stages appear as the most sensible choice. Indeed, the gain in efficiency with an additional two stages to S_n=8 is minor, while a restriction on the selected amount of turbine stages should be borne in mind. Indeed, the more stages, the more complex and large the turbine will be. Also, there are minimum dimensions to be respected. Indeed, it can be proven that a rise in stage count will result in a larger blade height, which may have an adverse effect on rotor parasite drag (see discussion on A_e conducted later). In addition, the negative effects of the increasing radius on the friction losses was not adopted in the model used to determine $\bar{r}_{i,opt}$, which would consequently yield too optimistic results while predicting the efficiency of the turbine.

The optimum specific inlet radius for the Diesel engine powered TDR cycle is slightly lower than the one found for Avgas engine powered TDR cycle (Table 4). Here, it is sufficient to mention that this effect is related to the slightly higher mass flow passing through the Diesel engine cycle to deliver the same RELT power output, since it operates at a lower cycle pressure ratio to achieve the same turbine inlet temperature[4].

TABLE 4 : OPTIMUM TURBINE SPECIFIC INLET RADIUS

			Avgas		Diesel	
LTIT	π_C	S_n [-]	$\bar{r}_{i,opt}$ [-]	$\eta_{is,T}$ / $\eta_{is,T}$ @ S_n=8	$\bar{r}_{i,opt}$ [-]	$\eta_{is,T}$ / $\eta_{is,T}$ @ S_n=8
all	*f(LTIT)*	4	0.210	0.81	0.220	0.93
all	*f(LTIT)*	6	0.180	0.98	0.175	0.98
all	*f(LTIT)*	8	0.170	1.00	0.170	1.00

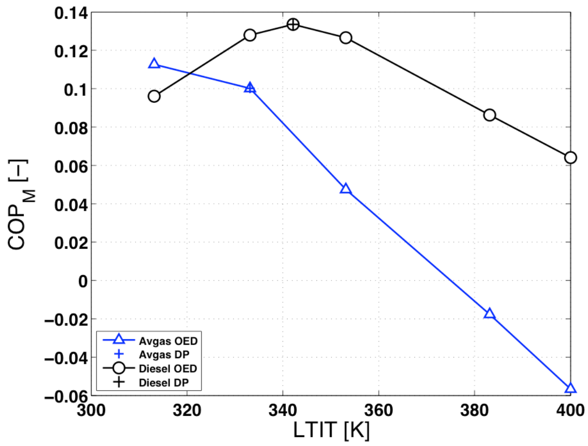

Fig.13 : *COP*-margin as a function of RELT inlet temperature (OED).

Now, it is possible to investigate COP_M for the found OED conditions as a function of turbine inlet temperature. For the Diesel engine powered cycle, a clear optimum exists near a turbine inlet temperature of 69°C (Fig.13), cycle pressure ratio of 1.24 (Fig.14) and mass flow rate of 4.9 kg/s. It has a COP_M of over 13%. This means that the TDR concept uses the invested energy better by the same amount over the conventional counterpart. The optimum originates from the positive impact of an increased *LTIT* on *COP*, becoming increasingly suppressed by the concurring increase in cycle pressure ratio, which affects the turbine polytropic efficiency negatively (Eq.2 and Fig.15). Note that the installed Diesel engine power then is 89 kW (ISA SLS).

An optimum COP_M was not retrieved for the Avgas engine in the examined temperature range, but the tendency on Fig.13 clearly shows that it is near or below 40°C. Pursuing these low temperatures appears unreasonable because the hub frontal drag would become prohibitively high, as indicated on Fig.16. Here the relative turbine frontal flow path area $A_{e,rel}$ is adopted as a drag metric, which can be related to the helicopter parasite drag as it contributes to the helicopter rotor equivalent flat plate area f_e[21]. The turbine frontal flow path area is defined as (Fig.17) :

$$A_e \triangleq {}^{L}H_{bo}{}^{L}R_o \propto f_e \qquad (35)$$

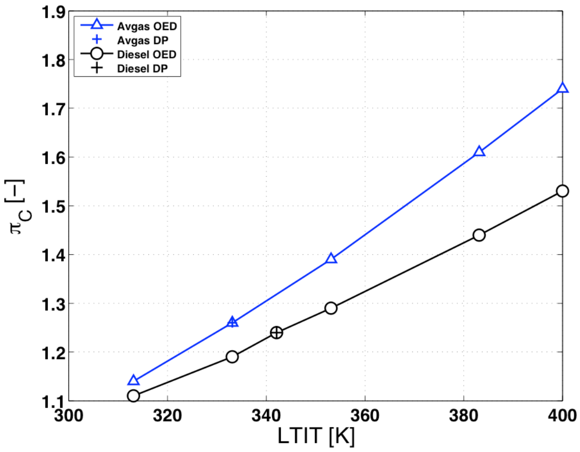

Fig.14 : Cycle pressure ratio as a function of RELT inlet temperature (OED).

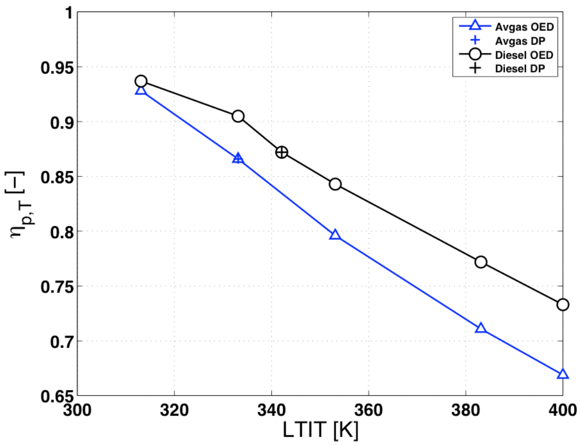

Fig.15 : RELT polytropic efficiency as a function of RELT inlet temperature (OED).

${}^{L}H_{bo}$ and ${}^{L}R_o$ are respectively the blade height and stage radius at the outlet of the last turbine stage. Note that the parasite drag is proportional to the square of the flight speed and should be accounted for in case high flight speeds are strived for.

For the piston powered TDR cycle, $A_{e,rel}$ is retrieved by the following relation :

$$A_{e,rel} = \frac{A_e}{\min(A_{e,range})} = \frac{A_e}{A_{e,400K}} \qquad (36)$$

The design point for the Avgas engine is selected at a COP_M of 10% (Fig.13), concurring with a turbine inlet temperature of 60°C and cycle pressure ratio of 1.26 (Fig.14). The mass flow rate is 4.7 kg/s. The selection of this configuration is found to be a reasonable compromise between a slight decrease in COP_M and a substantial reduction in $A_{e,rel}$ and thus drag (Fig.16). Note that the installed Avgas engine power is approximately 91.5 kW, which is very similar to the power required in the Diesel engine powered cycle.

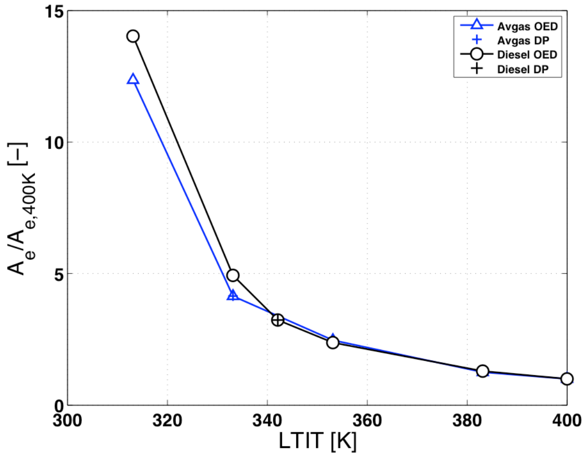

Fig.16 : Relative frontal flow path area $A_{e,rel}$ as a function of RELT inlet temperature (OED).

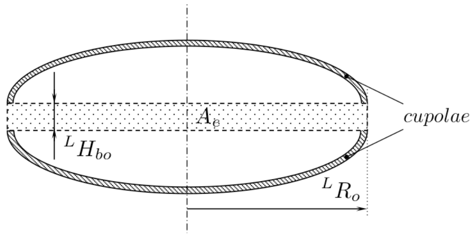

Fig.17 : Definition of the turbine frontal flow path area

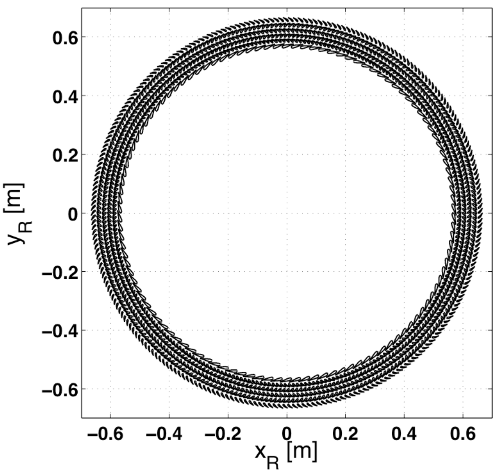

Fig.18 : Avgas engine powered TDR cycle, horizontal plane RELT cutaway.

The resulting design point RELT geometry for both the Avgas and Diesel engine powered cycles are very similar due to the comparable operating conditions. Hence, only the geometry of the Avgas engine powered TDR helicopter is presented in Figs. 18-20.

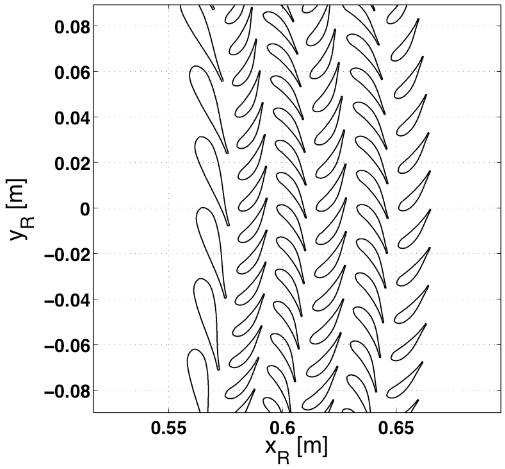

Fig.19 : Avgas engine powered TDR cycle, horizontal plane RELT cutaway : close-up.

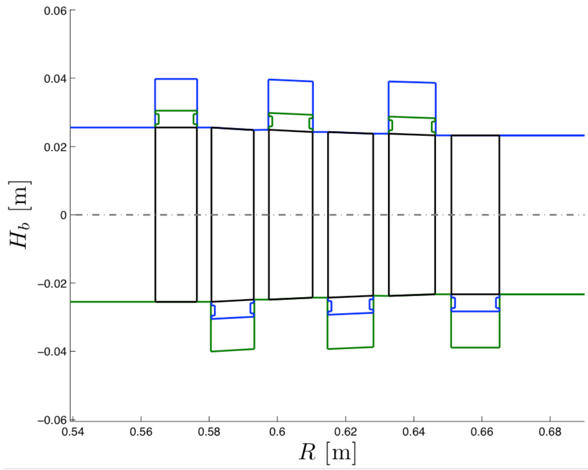

Fig.20 : Avgas engine powered TDR cycle, vertical plane RELT cutaway.

During the turbine development, a minimum design blade chord dimension of 2 cm was imposed, which is believed to be a reasonable size from a production perspective, while providing sufficient geometric accuracy (tolerances). From Fig.19 it is observed that the blades of the first stage are substantially larger than the ones in the subsequent stages. This can be explained by the rather high stagger angle at which these blades must be placed due to the imposed design criteria, but this phenomenon will not be further described here. Fig.20 highlights the slight reduction of the turbine blade height with turbine radius, which is necessary to compensate the effects of an increasing flow section. The axial distance between the rim and disk follows the design recommendation of Eq.16, yielding minimum torsional Couette friction losses. The notched rim works as a labyrinth seal, which reduces the leakage losses. Finally, Tables 5 & 6 summarise some important characteristics of the developed RELTs for the VLR-class TDR helicopter.

TABLE 5 : AVGAS ENGINE POWERED TDR CYCLE. RELT CHARACTERISTICS

Nominal operating conditions, ISA SLS

S_n	1	2	3	4	5	6
R_i [m]	0.564	0.581	0.598	0.615	0.633	0.651
c [mm]	41	22	23	23	24	21
Z [-]	114	266	266	266	266	249
ε [°]	13	82	82	82	82	71
$\eta_{p,T}$ [%]	86	87	87	87	86	87

c : blade chord -- Z : number of blades -- $n_{p,T}$: stage polytropic efficiency

TABLE 6 : DIESEL ENGINE POWERED TDR CYCLE. RELT CHARACTERISTICS

Nominal operating conditions, ISA SLS

S_n	1	2	3	4	5	6
R_i [m]	0.549	0.564	0.580	0.596	0.613	0.630
c [mm]	38	20	21	22	22	20
Z [-]	118	279	279	279	279	260
ε [°]	14	84	84	84	84	72
$\eta_{p,T}$ [%]	88	87	87	87	87	88

c : blade chord -- Z : number of blades -- $n_{p,T}$: stage polytropic efficiency

4.5. NH-90-class turbofan powered TDR cycle

4.5.1. Determination of COP_{BE}

Eq.29 tacitly assumed that the internal combustion engine generates a mechanical power P_M^*. This is not correct when using a turbofan, of which the single purpose is to deliver propulsive thrust. Hence, Eq.29 must be slightly modified. This is done by the introduction of the power gain PG[4], which is defined as :

$$PG \triangleq \frac{P_T^*}{T_{Nt}} \tag{37}$$

T_{Nt} is the total fictitious thrust delivered by the installed turbofan engine(s) in the TDR helicopter. Note that the thrust is indeed fictitious as the expansion of the gases leaving the turbofan is no longer governed by nozzles, but by the adiabatic RELT extracting energy instead. T_{Nt} is thus not delivered in reality and the actual propulsive forces generated by the engine are expected to be majorly suppressed by the upward deflection of the gases towards the RELT. Substitution of Eq.30 and Eq.37 in Eq.27, and using the definition of the turbofan thrust specific fuel consumption $TSFC = \dot{m}_f/T_{Nt}$, allows retrieving a break-even power gain :

$$PG_{BE} = \frac{TSFC}{SFC_{E,conv}}\left(1+\frac{\Delta W_E}{W_{g,conv}}\right)^b (1-k_{TX}-k_{TR})\, k_I \tag{38}$$

In case of the turbofan engine, Buysschaert et al.[4] defined the coefficient of performance of the turbofan differently than the one for the engines delivering mechanical power directly, i.e. :

$$COP_{TF} \triangleq \frac{P_T^*}{\dot{E}_k} \tag{39}$$

where $\dot{E}_k$ represents the kinetic energy added by the turbofan engine to the gases. It is then possible to establish the break-even coefficient of performance based on the break-even power gain :

$$COP_{BE} = \frac{2}{SPT}\left(1+\frac{FAR}{1+BPR_{TF}}\right) PG_{BE} \tag{40}$$

For the current evaluation, the turbofan turbine inlet temperature TIT is set to 1600 K[22], while - based on a data survey performed by the authors - the overall pressure ratio OPR is set to 32. This makes the gas turbine cycle study a pure function of BPR_{TF}. This study is conducted using the GasTurb 11 software of Joachim Kurzke (MTU). Subsequently, correlations for SPT, $TSFC$, and the RELT inlet total pressure and temperature as a function of BPR_{TF} are retrieved and introduced in the parametric TDR cycle study, where BPR_{TF} is used as the sole independent variable.

At this point, the remaining unknown parameter is the change in empty weight with respect to the conventional helicopter ΔW_E. For the turbofan powered TDR cycle, it is quantified as :

$$\begin{aligned}\Delta W_E \approxeq W_{E,T} + W_{E,TF} + \Delta W_{E,2} - W_{E,3A} \ldots \\ -W_{E,7A} - W_{E,7B}\end{aligned} \tag{41}$$

In the foregoing equation, $W_{E,TF}$ represents the weight of the turbofan, which is a function of the maximum take-off thrust at ISA SLS conditions (Fig.21). In contrast to Eq.32, the weight of the powerplant system (piston engine or turboshaft) $\Delta W_{E,7A}$ must be subtracted too because of the installation of the turbofan, while no weight needs to be added for a compressor $W_{E,C}$, as the fan of the turbofan engine already accomplishes the function of the former. Note that since it is a NH-90-class TDR helicopter, the conventional helicopter gross weight $W_{g,conv}$ was set equal to 10600 kg.

For a given BPR_{TF}, the turbofan "fictitious" thrust that needs to be selected to drive the RELT then depends on the required power P_T^* and mass flow, and the acquired turbine polytropic efficiency. The solution must be sought iteratively by coupling the cycle performance model with the RELT model. Note that if the cycle pressure ratio and turbine expansion ratio are assumed identical, which is a first order approximation, and if in addition the turbine polytropic efficiency is examined independently, which boils down to leaving the turbine model out of consideration, it is possible to estimate the break-even coefficient of performance and power gain (Fig.22).

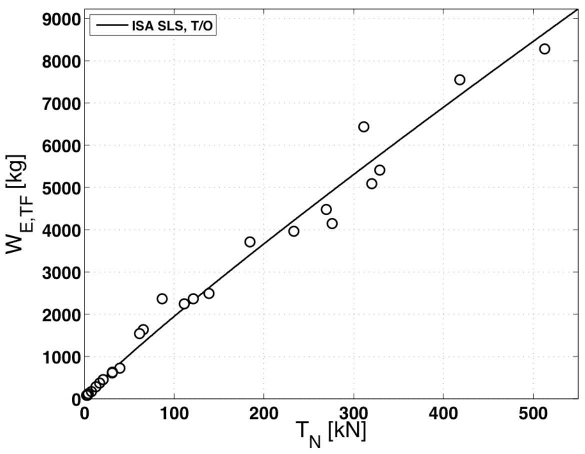

Fig.21 : Turbofan weight as a function of maximum take-off thrust (ISA SLS, from author survey).

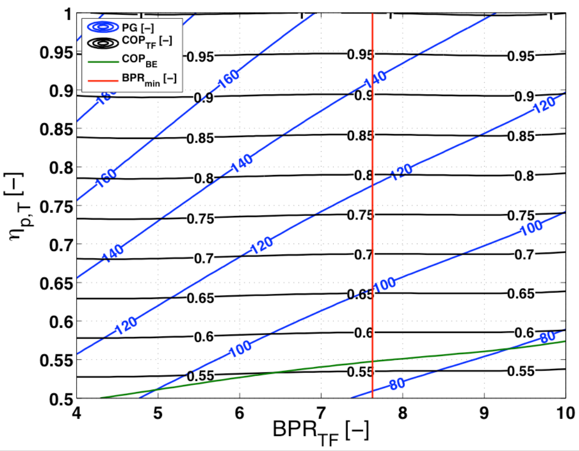

Fig.22 : Turbofan powered TDR cycle, estimation of power gain and coefficient of performance (ISA SLS).

For the examined helicopter configuration, $W_{g,TDR} / W_{g,conv}$ can be shown to be approximately 93%. From Fig.22, it is concluded that :

$$PG_{BE} \approxeq 80 \tag{42}$$

$$COP_{BE} \approxeq 0.57 \tag{43}$$

This concurs with a RELT polytropic efficiency of approximately 57%. For the nominal operating condition, this efficiency will be observed to be significantly higher. Note that there exists a lower boundary to the selection of BPR_{TF}, caused by the maximum allowable $LTIT$, which is 400 K. The resulting geometry and performance characteristics achieved by coupling the turbine model with the cycle model for a range of bypass ratios, are treated next.

4.5.2. Cycle and turbine matching

By analogy with the methodology discussed in Section 4.4.2, the optimum specific inlet radius and stage number yields a RELT with the highest possible efficiency (OED). Based on the correlations of Buysschaert et al.[1], the helicopter rotor tip radius is 8.3 m, which leads to a turbine angular velocity approximately 249 RPM. The required power then is 1.35 MW per crown (Fig.8). Table 7 summarises important design aspects regarding the number of stages and the absolute middle stage inlet flow angle. Note that only the values for BPR_{TF} = 8 are given, as the parametric study on the selection of the turbofan bypass ratio shows that it is the optimum choice for a maximum coefficient of performance margin (Fig.23). While the number of stages increases the turbine efficiency, the turbine frontal flow path area A_e becomes important (Table 7).

TABLE 7 : OPTIMUM TURBINE SPECIFIC INLET RADIUS AND IMPACT OF MIDDLE STAGE ABSOLUTE INLET FLOW ANGLE

BPR [-]	π_T [-]	${}^{M}\alpha_i$ [°]	S_n [-]	$\bar{r}_i$ [-]	$\eta_{is,T}$ [-]	A_e / A_e^* [-]	OED
8	1.502	65	4	0.32	0.89	1.98	yes
8	1.507	65	6	0.30	0.92	2.86	yes
8	1.510	65	8	0.29	0.94	3.67	yes
8	1.472	6	40	0.27	0.91	1.16	yes
8*	1.444*	6*	40*	0.20*	0.90*	1*	no*

" * " represents the selected design conditions

As highlighted earlier in this paper, this can become problematic at the higher speeds, due to rotor parasite drag concerns. Selecting a stage number of 6 and reducing the middle stage inlet flow angle to 40° then appears as a reasonable compromise between turbine efficiency and parasite drag reduction. Because COP_M shows to be sufficiently large (Fig.23), it was decided to further reduce the turbine efficiency slightly (1%) to prune the frontal flow path area with another 16%. This was achieved by reducing $\bar{r}_i$ to a value of 0.20. COP_M then still is 47%. Note that the mass flow at the selected design point is around 75 kg/s, while the power gain approximately 120. For the delivered power, this means that the to-be-selected installed take-off thrust of the turbofan is approximately 22.5 kN (ISA SLS). This is certainly within the range of possibilities of a single turbofan engine.

Note that with regard to Fig.24, the relative frontal flow path area is defined here as :

$$A_{e,rel} = \frac{A_e}{\min(A_{e,range})} = \frac{A_e}{A_{e,BPR_{TF}=4}} \tag{44}$$

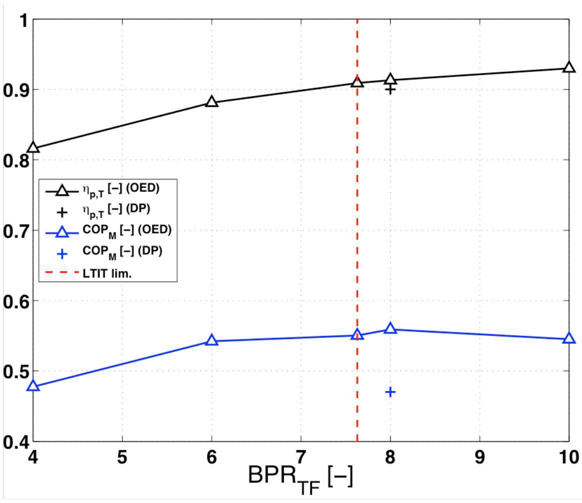

Fig.23 : Turbofan powered TDR cycle COP_M and turbine polytropic efficiency as a function of turbofan bypass ratio.

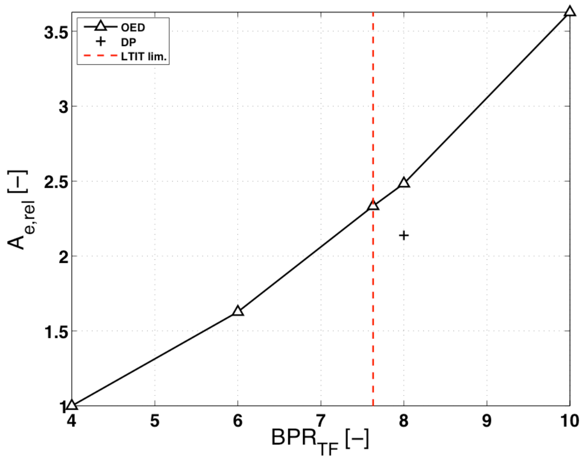

Fig.24 : Relative frontal flow path area $A_{e,rel}$ as a function of RELT inlet temperature.

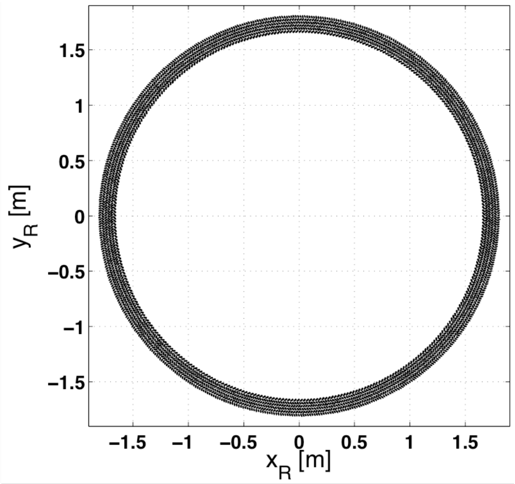

Fig.25 : Turbofan engine powered TDR cycle, horizontal plane RELT cutaway.

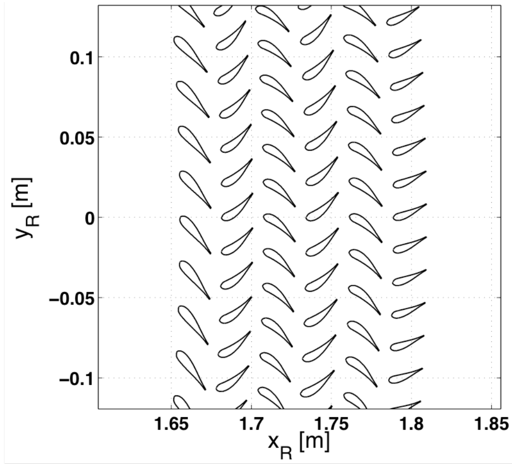

Fig.26 : Turbofan engine powered TDR cycle, horizontal plane RELT cutaway : close-up.

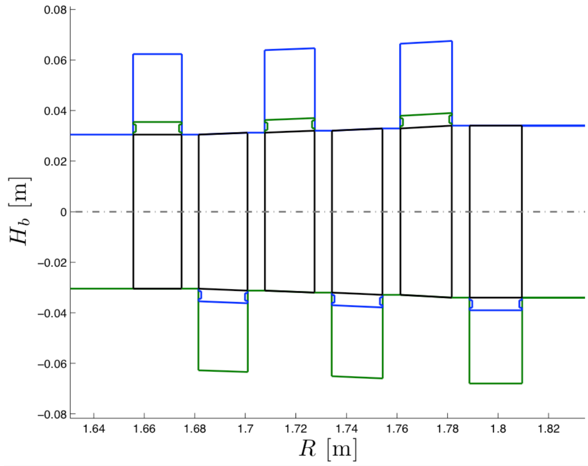

Fig.27 : Turbofan engine powered TDR cycle, vertical plane RELT cutaway

Since the turbine blade stagger angle of the first stage in the turbofan powered TDR cycle is roughly 25° lower than the one observed in the RELT designed for the piston engine powered TDR cycles, the size of the blades of the first stage does not differ largely from those in the subsequent stages (Figs. 25 & 26). This difference is due to the decreased middle stage inlet flow angle, imposed to diminish the negative effects of rotor parasite drag.

The minimum blade chord length of approximately 20 mm was again imposed as the lower boundary in the design procedure, as it generally engenders lower turbine losses (Section 3.3 & 3.4). Note that in contrast to the piston engine powered cycles, the blade height in the RELT of the turbofan powered cycle increases with turbine radius (Fig.27). The higher Mach numbers observed in the latter cause the compressibility effects to become more pronounced (effect on flow density), which explains this phenomenon. Slightly higher stage efficiencies are also observed (Table 8), which can be attributed to the increased mass flow, influencing the blade aspect ratio and flow Reynolds number positively

TABLE 8 : TURBOFAN ENGINE POWERED TDR CYCLE. RELT CHARACTERISTICS

Nominal operating conditions, ISA SLS

S_n	1	2	3	4	5	6
R_i [m]	1.656	1.682	1.708	1.734	1.761	1.789
c [mm]	30	24	25	25	26	22
Z [-]	372	497	497	497	497	555
ε [°]	27	73	73	73	73	46
$\eta_{p,T}$ [%]	88	90	90	90	90	93

c : blade chord -- Z : number of blades -- $\eta_{p,T}$: stage polytropic efficiency

5. CONCLUSIONS

In this paper, the design and integration methodology of a rotor embedded Ljungström turbine has been realised.

The discussion highlighted the importance of an integrated approach of the TDR helicopter performance optimisation by matching the cycle and turbine thermodynamic parameters optimally. For this purpose, the break-even coefficient of performance was defined.

In this paper, the A_3K_7 turbine blade was selected because it is reported to be suitable for high reaction turbines. The foregoing criterion is applicable to the rotor embedded Ljungström turbine.

A design methodology using the model of Soderberg and considering disk friction and leakage losses was proposed and used to retrieve the Ljungström turbine specific inlet radius yielding maximum efficiency (OED).

The OED results were evaluated parametrically for a VLR-class TDR helicopter, using either an Avgas or a Diesel reciprocating engine, and a NH-90-class TDR helicopter using a turbofan. For the piston engine powered TDR cycle, the Diesel engine appears to hold a performance margin of approximately 13% over the conventional helicopter. For the Avgas engine configuration, this margin was slightly lower (10%), as it was decided to sacrifice part of it in order to assure a lower impact of the Ljungström turbine on the rotor parasite drag, but still of comparable magnitude as found with the Diesel engine configuration. With regard to the turbofan powered TDR cycle, the installation of a turbofan engine engenders a coefficient of performance margin of approximately 47%. The all above-mentioned values apply to the nominal operating regime ISA SLS, while using a six-stage Ljungström turbine as it showed to be the best compromise between high turbine efficiency and a low parasite drag impact.

It is important to emphasise that the design point should normally be examined as a function of the design flight profile, which was not considered here. Then, only better guidance on the selection of the optimal turbine frontal flow path area will be possible, since the design speed and altitude plays a vital role on the importance of rotor parasite drag.

While the nominal operating regime gives satisfactory performance values for the TDR helicopter concept with regard to the conventional helicopter, it should still be evaluated against off-design operating regimes, which are usually an important part of the flight profile. This examination is involved and should be adopted in a dynamic model of the complete system. Further research in this domain is recommended.

6. REFERENCES

[1] F. Buysschaert, P. Hendrick, and S. Newman, “Conventional helicopters: an adaptiveness study for more electric and alternative propulsion technologies,” *Journal of Aerospace Engineering*, vol. 226, pp. 1078–1094, 2011.

[2] H. Antoine, G. Dimitriadis, P. Hendrick, E. Kagambage, and T. Rayee, “A novel concept for helicopter rotor drives,” in *3rd European Conference for Aero-Space Sciences*, (Versailles, Paris, France), July 6-9 2009.

[3] F. Buysschaert, S. Newman, S. Walker, H. Antoine, and P. Hendrick, “The Ljungström turbine for aeronautical applications,” in *5th European Conference for Aeronautics and Space Sciences*, (München), EUCASS, July 2013.

[4] F. Buysschaert, S. Newman, S. Walker, H. Antoine, and P. Hendrick, “The turbine driven rotor concept, a new vision for helicopter propulsion,” in *40th European Rotorcraft Forum*, (Southampton, United Kingdom), September 2014.

[5] J. Horlock. Axial Flow Turbines : *Fluid mechanics and thermodynamics*. Butterworths, London, United Kingdom, 1966.

[6] R. H. Aungier. *Turbine Aerodynamics*. Axial-flow and radial-inflow turbine design and analysis. ASME press, 2006.

[7] J. Daily and R. Nece. Chamber dimension effects on induced flow and frictional resistance of enclosed rotating disks. *Journal of Basic Engineering*, 82(1):217-230, March 1st 1960.

[8] S. Haddadi and S. Poncet. Turbulence modeling of torsional Couette flows. *International Journal of Rotating Machinery*, 2008:27, 2008.

[9] J. Goulburn and J. Wilson. High speed disk friction losses in a gaseous medium. *International Journal of Mechanical Sciences*, 17(6):379-382, 1975.

[10] H. S. Dou, B. C. Khoo, and K. S. Yeo. Instability of Taylor-Couette flow between concentric rotating cylinders. *International Journal of Thermal Sciences*, (47):1422–1435, 2008.

[11] Y. Çengel and J. Cimbala. *Fluid Mechanics : Fundamentals and Applications*. McGraw-Hill, Inc, New York, USA, 2nd edition, 2010.

[12] D. Eser and Y. Dereli. Comparisons of rotordynamic coefficients in stepped labyrinth seals by using Colebrook-White friction factor model. *Meccanica*, 42:177-186, 2007.

[13] R. Shaw. Efficiency predictions for axial-flow turbines. *International Journal of Mechanical Sciences*, 8(3):171-192, 1966.

[14] R. Malvano, F. Vatta, and A. Vigliani. Rotordynamic coefficients for labyrinth gas seals: single control volume model. *Meccanica*, 36:731-744, 2001.

[15] D. Eser and J. Y. Kazakia. Air flow in cavities of labyrinth seals. *International Journal for Engineering Sciences*, 33(15):2309-2325, 1995.

[16] K. Neumann. Zur Frage der Verwendung von Durchblickdichtungen im Dampfturbinenbau. *Maschinentechnik*, 13(4), 1964.

[17] C. P. Coleman. A survey of theoretical and experimental coaxial rotor aerodynamic research. Technical paper 3675, National Aeronautics and Space Administration, March 01, 1997.

[18] W. Johnson. *Helicopter theory*. Dover publications, inc., 1994.

[19] J. Leishman. *Principles of Helicopter Aerodynamics*. Cambridge University Press, 2002.

[20] M. N. Beltramo and M. A. Morris. Parametric study of helicopter aircraft systems costs and weights. NASA CR-152315, January 1980.

[21] R. Prouty. *Helicopter Performance, Stability and Control*. Krieger, 2002.

[22] N. Cumpsty. *Jet Propulsion : a simple guide to the aerodynamic and thermodynamic design and performance of jet engines*. Cambridge University Press, 2000.